HHS Public Access

Author manuscript

J Comp Neurol. Author manuscript; available in PMC 2023 December 01.

Published in final edited form as:

J Comp Neurol. 2022 December ; 530(18): 3179–3192. doi:10.1002/cne.25401.

The parabigeminal nucleus is a source of "retinogeniculate replacement terminals" in mice that lack retinofugal input

Kyle L. Whyland[1], **Yanio Hernandez**[1], **Arkadiusz S. Slusarczyk**[1], **William Guido**[1], **Martha E. Bickford**[1,*]

[1]Department of Anatomical Sciences and Neurobiology, University of Louisville, Louisville, KY 40292

Abstract

In the dorsal lateral geniculate nucleus (dLGN) of mice that lack retinal input, a population of large terminals supplants the synaptic arrangements normally made by the missing retinogeniculate terminals. To identify potential sources of these "retinogeniculate replacement terminals", we used mutant mice (*math5*$^{-/-}$) which lack retinofugal projections due to the failure of retinal ganglion cells to develop. In this line, we labeled dLGN terminals that originate from the primary visual cortex (V1) or the parabigeminal nucleus (PBG), and compared their ultrastructure to retinogeniculate, V1 or PBG terminals in the dLGN of C57Blk6 (WT) mice. Corticogeniculate terminals labeled in WT and *math5*$^{-/-}$ mice were similar in size and both groups were significantly smaller than WT retinogeniculate terminals or labeled PBG terminals in the dLGN of either mouse line. To examine projections from cortical layer V, we labeled V1 projections in a cre-dependent manner in RpB4-cre and RpB4-cre/*math5*$^{-/-}$ mice; in both lines labeled V1 axons coursed through the dLGN but few labeled synaptic terminals were observed. Additionally, no changes in the overall WT distribution of tectal or peduculopontine projections were detected in the dLGN of *math5*$^{-/-}$ mice. However, the PBG projection in *math5*$^{-/-}$ mice was extensive and there was considerable overlap in the sizes of retinogeniculate terminals in WT mice and PBG terminals in *math5*$^{-/-}$ mice. The data indicate that V1 is not a source of "retinogeniculate replacement teminals" and suggests that large PBG terminals expand their innervation territory to replace retinogeniculate terminals in their absence.

Graphical Abstract

In the dorsal lateral geniculate nucleus (LGN) of mice that lack retinal input, a population of large terminals supplants the synaptic arrangements normally made by the missing retinogeniculate terminals. To identify potential sources of these "retinogeniculate replacement terminals", we used mutant mice (*math5*$^{-/-}$) which lack retinofugal projections due to the failure of retinal ganglion cells to develop. In this line, we labeled LGN terminals that originate from the primary

*Corresponding author: address: 511 S. Floyd St. Louisville, KY 40292, martha.bickford@louisville.edu.

Author contributions: **Kyle Whyland:** Conceptualization, Investigation, Formal Analysis, Visualization, Writing (Original Draft Preparation, Review and Editing), Funding Acquisition **Yanio Hernandez:** Investigation, Formal Analysis **Ark Slusarczyk:** Methodology, Investigation **Willam Guido:** Resources, Writing (Review & Editing), Funding Acquisition **Martha Bickford:** Project Administration, Conceptualization, Investigation, Visualization, Writing (Original Draft Preparation, Review and Editing), Funding Acquisition.

Conflict of interest: The authors declare no competing financial interests.

visual cortex (V1) or the parabigeminal nucleus (PBG), and compared their ultrastructure to retinogeniculate, V1 or PBG terminals in the dLGN of C57Blk6 (WT) mice (schematically depicted above graph). Corticogeniculate terminals labeled in WT and *math5*$^{-/-}$ mice were similar in size and both groups were significantly smaller than WT retinogeniculate terminals. In contrast, the PBG projection in *math5*$^{-/-}$ mice was extensive and there was considerable overlap in the sizes of retinogeniculate terminals in WT mice and PBG terminals in *math5*$^{-/-}$ mice (summarized in histogram). The data indicate that V1 is not a source of "retinogeniculate replacement terminals" and suggests that large PBG terminals expand their innervation territory to replace retinogeniculate terminals in their absence.

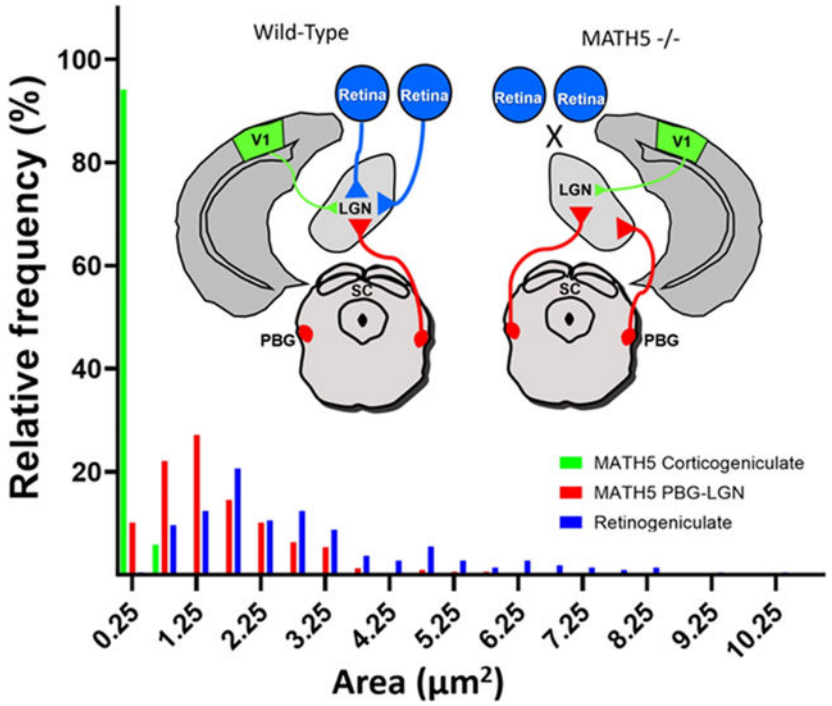

Keywords

dorsal lateral geniculate nucleus; synapse; ultrastructure; corticogeniculate; tectogeniculate; pedunculopontine tegmentum; *math5*$^{-/-}$; RpB4-cre

Introduction

Vision loss early in life, or as a consequence of adult-onset disease or trauma has a major impact on the form and function of retino-recepient targets in the brain (Ptito et al., 2021). For example in the dorsal lateral geniculate nucleus (dLGN, the thalamic relay of retinal signals en route to the visual cortex), the absence or elimination of retinal input leads to a number of degenerative effects including an overall skrinkage of the dLGN, a loss of dLGN neurons, a reduction in soma size as well as a decrease in the dendritic complexity of remaining neurons (Abbott et al., 2015; Bhandari et al., 2022; El-Danaf et al., 2015; Gupta et al., 2009). While these studies have focused largely on the structural integrity and cellular composition of the dLGN, recent evidence suggests that the vision loss also

alters the connectivity between the dLGN and central structures that do not receive retinal input (Brooks et al., 2013; Frangeul et al., 2016; Giasafaki et al., 2022; Grant et al., 2016; Seabrook et al., 2013; Sokhadze et al., 2018). Indeed, a deeper understanding of these axon target interactions, especially at the ultrastructural level, is a critical first step in developing effective treatments for the restoration of vision following disease or trauma (Goldberg et al., 2016).

Retinal ganglion cells normally innervate the dLGN with large terminals that contain round vesicles and pale mitochondria (RLP profiles; Bickford et al., 2010; Hammer et al., 2015). Synaptic profiles exhibiting this ultrastructure are missing in congenitally anophthalmic mice (Cullen & Kaiserman-Abramof, 1976; Kaiserman-Abramof, 1983), microphthalamic mice (Winkelmann et al., 1985), enucleated mice (Cullen & Kaiserman-Abramof, 1976; Kaiserman-Abramof, 1983), or mice in which retinal ganglion cells fail to develop and lack retinofugal projections (El-Danaf et al., 2015). In the absence of RLP profiles, these previous ultrastructural studies have noted the presence of large terminals in the dLGN that appear to assume the location and synaptic targets of the missing retinal terminals. In particular, except for the fact that these terminals contain dark mitochondria, these “retinal replacement terminals” exhibit most of the ultrastructural features of retinogeniculate terminals, i.e. large size, round synaptic vesicles, synaptic contacts on the dendrites of thalamocortical relay cells (including dendritic protrusions) and the dendrites of interneurons (including dendritic terminals or F2 profiles; Bickford et al., 2010; Hammer et al., 2015; Morgan & Lichtman, 2020). However, the source of these terminals remains unclear.

In the absence of retinal input, two sources of replacement terminals have been suggested. First, it has been reported that axons of layer V cortical neurons abberantly innervate the dLGN following enucleation (Grant et al., 2016), and could potentially assume the morphology of retinal terminals. It has also been reported that projections from the midbrain parabigeminal nucleus (PBG) to the dLGN increase following enucleation and may assume the morphology of retinal terminals (Stevenson & Lund, 1982). An expansion of projections from the PBG to the dLGN has also been observed in a mutant mouse line that lacks *math5*, a transciption factor needed for the differentiation of retinal ganglion cells from progenitors. As a result, retinal ganglion cells fail to develop in *math5*$^{-/-}$ mice, an optic nerve does not develop, and these mice lack retinofugal projections (Charalambakis et al., 2019; El-Danaf et al., 2015; Seabrook et al., 2013; Sokhadze et al., 2018; Wang et al., 2001). In this line, PBG projections expand to fill both the ipsilateral and contralateral dLGN (Sokhadze et al., 2018). To test whether the cortex and/or the PBG are the source or retinogeniculate replacement terminals in *math5*$^{-/-}$ mice, we compared the ultrastructure of geniculate terminals that originate from the cortex or PBG labeled in this line with geniculate terminals that originate from the retina, cortex or PBG labeled in wild type (WT) mice with intact retinal projections.

Methods

All breeding and experimental procedures were approved by the University of Louisville Institutional Animal Care and Use Committee. Experiments were carried out using mice, of

either sex, of C57BL/6J (IMSR Cat# JAX_000664, RRID: IMSR_JAX:000664), a line in which most layer five, and a subset of layer six, cortical neurons express Cre-recombinase (Tg(Rbp4-cre)KL105Gsat; RRID: MMRRC_036400-UCD), a line that fails to develop an optic nerve or retinofugal pojections due to a >95% loss of retinal ganglion cells during early development (*math5* $^{-/-}$; El-Danaf et al., 2015; Seabrook et al., 2013; Wang et al., 2001; RRID: MMRRC_042298-UCD), and *math5*$^{-/-}$ mice crossed with Rbp4-cre mice.

Tracer and virus injections

To label projections from the cortex, parabigeminal nucleus (PBG), or superior colliculus (SC), adult mice (median age postnatal day 47) were deeply anesthetized with a mixture of ketamine (100–150 mg/kg) and xylazine (10–15 mg/kg). The analgesic meloxicam (5 mg/kg) was also injected prior to surgery. The animals were then placed in a stereotaxic apparatus (Angle Two Stereotaxic, Leica, Wetzlar, Germany). An incision was made along the scalp, and a small hole was drilled in the skull overlying the primary visual cortex (V1; 3.4 mm caudal to Bregma, 2.4 mm lateral to midline, 1.15 mm ventral to Bregma), the PBG (4.3 mm caudal to Bregma, 1.85 mm lateral to midline, 3.2 mm ventral to Bregma), or the SC (3.75 mm caudal to Bregma, 0.6 mm lateral to midline, 1.3 mm ventral to Bregma). Adeno-associated viruses (AAVs; AAV1-DIO-Matrix-dAPEX2, gift from David Ginty; Addgene plasmid #117177; RRID: Addgene_117177); AAV1-Matrix-dAPREX2 (Addgene plasmid# 117176; RRID: Addgene_117176), AAV9-Ef1a-DIO-dAPEX2 (Addgene plasmid #117174; RRID: Addgene_117174), AAV8.2-DIO-mCherry-WPRE (RRID: Addgene_50459-AAV8), pAAV1-CAG-GFP (RRID: Addgene_37825-AAV1), or the tracer biotinylated dextran amine (BDA, Invitrogen) were injected unilaterally in V1, PBG, or the SC. For BDA injections, a glass pipette (10 μm tip diameter) containing a 5% solution of BDA in saline was lowered into V1, and BDA was iontophoretically ejected using 3 μA continuous positive current for 20 min. The viruses were delivered via a 34-gauge needle attached to a Nanofil syringe inserted in an ultramicropump. The needle was lowered into V1, PBG or the SC and volumes of 70–120 nl were injected at a rate of 30 nl/min. After removal of the pipette or needle, the scalp skin was sealed with tissue adhesive (n-butyl cyanoacrylate), and the animals were placed on a heating pad until mobile. Post-surgery, animals were carefully monitored for proper wound healing, and meloxicam (5 mg/kg) was administered for 48 hours.

To label projections from the retina, C57Blk6 pups (p15–18) received unilateral intravitreal injections of AAV1-Matrix-dAPREX2. Each pup was anesthetized with isoflurane via a small nose cone, the sclera was pierced with a sharp-tipped glass pipette, and excess vitreous was drained. Another pipette filled with the AAV solution was inserted into the hole made by the first pipette. The pipette containing the AAV was attached to a picospritzer and a volume of approximately 1 μl of solution was injected into the eye. The nose cone used to administer isoflurane was then removed and, once alert, the pup was returned to the cage containing the dam and littermates.

Electron microscopy (V1, PBG and retinogeniculate terminal ultrastructure)

One week following BDA injections, two weeks following V1 or PBG virus injections, and two-three weeks after intravitreal injections, mice were transcardially perfused with 2% paraformaldehyde and 2% glutaraldehyde in 0.1M phosphate buffer at pH 7.4 (PB). The brains were removed from the skull and placed in the fixative solution overnight at 4°C. The next day, the brains were cut using a vibratome into coronal sections at a thickness of 70 μm. Sections from virus-injected animals were reacted with nickel-enhanced diaminobenzidine (DAB) immediately after sections were cut to prevent loss of enzyme activity. Sections from BDA-injected animals were placed overnight in a solution of avidin and biotinylated horseradish peroxidase (ABC solution, Vector Laboratories). The following day, after rinsing in PB, the sections were reacted with nickel-enhanced DAB.

Sections that contained DAB-labeled axons and terminals were postfixed in 2% osmium tetroxide, dehydrated in an ethyl alcohol series, and flat embedded in Durcupan resin between two sheets of Aclar plastic (Ladd Research, Williston, VT). Durcupan–embedded sections were first examined with a light microscope to select areas for electron microscopic analysis. Selected areas were mounted on blocks, ultrathin sections (60–80 nm, silver-gray interference color) were cut using a diamond knife, and sections were collected on Formvar-coated nickel slot grids. Selected sections were stained for the presence of GABA. A postembedding immunocytochemical protocol described previously (Bickford et al. 2010; Zhou et al. 2018; Masterson et al. 2019) was employed. Briefly, we used a 0.25 μg/ml concentration of a rabbit polyclonal antibody against GABA (Sigma-Aldrich, St. Louis, MO, catalogue #A2052, RRID:AB_477652, immunogen was GABA conjugated to bovine serum albumin using glutaraldehyde; the GABA antibody shows positive binding with GABA and GABA-keyhole limpet hemocyanin, but not bovine serum albumin, in dot blot assays; manufacturer's product information). In mouse tissue, the GABA antibody stains most neurons in the thalamic reticular nucleus and a subset of neurons in the dorsal thalamus and cortex. This labeling pattern is consistent with other GABAergic markers used in a variety of species (Fitzpatrick et al., 1984; Houser et al., 1980; Montera & Zempel, 1985; Montero & Singer, 1984). The GABA antibody was tagged with a goat-anti-rabbit antibody conjugated to 15-nm gold particles (BBI Solutions USA, Madison, WI, catalogue# GAR12/0.25, RRID:AB_1769132). The sections were air dried and stained with a 10% solution of uranyl acetate in methanol for 30 minutes before examination with an electron microscope.

Images of DAB-labeled terminals involved in synapses were collected and the areas of the presynaptic profiles were measured using ImageJ software (RRID: SCR_002285). Other ultrastructural features, such as the presence or absence of dendritic inclusions within terminals, were noted. For presentation of ultrastructural features, electron microscopic images were imported into Adobe Photoshop software (San Jose, CA), and the brightness and contrast were adjusted.

Confocal microscopy (tectogeniculate and cholinergic terminal distributions)

Two weeks following SC virus injections, mice were transcardially perfused with 4% paraformaldehyde in PB. The brains were removed from the skull and placed in the

fixative solution overnight at 4°C. The next day, the brains were cut using a vibratome into coronal sections at a thickness of 70 μm, mounted on slides, and imaged using a confocal microscope.

Cholinergic brainstem projections to the dLGN were labeled via immunohistochemistry using brain sections from mice prepared as described above. Selected sections were washed with 0.3% Triton X-100 and 10% normal donkey serum (NDS) in phosphate buffered saline (PBS; 0.01M phosphate buffer with 0.9% NaCl) for 1 h, and incubated overnight (12 h) in a 1:100 dilution of a rabbit polyclonal antibody against vesicular acectylcholine transporter (vAChT; Synaptic Systems Cat# 139103, RRID: 887864) in 1% NDS in PBS. The immunogen for this antibody was a recombinant protein corresponding to AA 475 to 530 from rat VAChT. The neurons and boutons labeled with this antibody correspond to those labeled previously using choline acetyl transferase antibodies (Deichler et al., 2020; Sokhadze et al., 2022; Steinkellner et al., 2019). Following incubation in the VAChT antibody, the next day sections were incubated in a 1:100 dilution of a donkey-anti-rabbit antibody directly conjugated to a fluorescent compound, Alexa Fluor 647 (Cat#A32849, RRID: AB_2762840) for 1 h. After three rinses with PB for 10 min each, the sections were mounted on slides and imaged using a confocal microscope. Confocal images of SC projections and VAChT labeling were imported into Adobe Photoshop and inverted. The brightness and contrast were adjusted, and bubbles or other imperfections were removed to optimize presentation.

Material collected in previous studies

Measurements of BDA-labeled corticogeniculate terminals labeled in C57BL/6J mice, and images of the distribution of tectogeniculate terminals and VAChT terminals in C57BL/6J mice were previously collected and published (Bickford et al., 2015; Sokhadze et al., 2022).

Statistical analysis

GraphPad Prism (RRID: SCR_002798) was used for statistical analysis. For all results involving comparisons of more than two groups, Kruskal-Wallis tests were used to determine whether terminal sizes were significantly different. All graphs featured in the figures of the results section were produced with GraphPad Prism.

Results

Electron microscopy was used to obtain images of virus- or tracer-labeled terminals in the dLGN that were involved in synaptic connections. Retinogeniculate terminals (in wild type mice with intact retinal ganglion cells) were identified as profiles in which all mitochondria were labeled with a dark reaction product (Figure 1a,b). For all other projections, the tracer or virus injections resulted in a dark reaction product that filled the cytoplasm of axons and synaptic terminals with a dark reaction product which surrounded synaptic vesicles (Figures 2, 5 and 7).

Retinogeniculate terminals in WT mice

As previously described (Bickford et al., 2010), mouse retinogeniculate terminals were large profiles that synapse on the nonGABAergic dendrites of relay cells (Figure 1a,b, green) and the GABAergic dendritic terminals of interneurons (F2 profiles; Figure 1b, red). Postsynaptic dendrites often protruded into the retinogeniculate terminals (Figure 1a,b). For measurements of retinogeniculate profiles, any dendritic protrusions enclosed within the terminal profile were included in the area measurements. We found no significant difference in the sizes of virus-labeled retinogeniculate terminals ipsilateral (n = 113 synaptic terminals; 2.956 ± 1.868 μm^2) or contralateral (n = 105 synaptic terminals; 2.798 ± 2.028 μm^2) to the injected eye (Figure 3; Kruskal-Wallis, $p > 0.9999$). There was also negligible differences in the proportion of synapses on relay cells (ipsilateral 88%; contralateral 87%) and interneurons (ipsilateral 12%; contralateral 13%), or in the proportion of retinogeniculate terminals that contained dendritic protrusions (38.5% of ipsilateral terminals contained protrusions; 34% of contralateral terminals contained protrusions).

Corticogeniculate terminals in WT, math5$^{-/-}$, RPB4-cre and RPB4-cre/math5$^{-/-}$ mice

Following perinatal monocular enucleation, cortical inputs to the dLGN arise exclusively from V1 (Giasafaki et al., 2022; Grant et al., 2016). Thus, we labeled corticogeniculate terminals via V1 BDA injections in wild type and *math5*$^{-/-}$ mice. Our injections encompassed all cortical layers to include layer VI neurons that are normally the exclusive source of cortical input to the dLGN (Augustinaite & Kuhn, 2020), as well as layer V neurons which have been reported to abberantly innervate the dLGN after early postnatal monocular enucleation (Giasafaki et al., 2022; Grant et al., 2016). As previously described (Bickford et al., 2015) in wild type mice, corticogeniculate terminals are small profiles (n = 74 synaptic terminals; 0.178 ± 0.0847μm^2) with densely-packed round vesicles (RS profiles; Figure 2a). In mice devoid of retinal input (*math5*$^{-/-}$), corticogeniculate terminals labeled via V1 BDA injections were also found to be RS profiles (Figure 2b–d; n = 240 synaptic terminals; 0.238 ± 0.123 μm^2) that were similar in size to WT corticogeniculate terminals (Figure 3; Kruskal-Wallis, $p = 0.0542$). In both WT and *math5*$^{-/-}$ mice, corticogeniculate terminals were found to be significantly smaller than retinogeniculate terminals in wild type mice (Figure 3; Kruskal-Wallis, $p < 0.0001$). We also found that corticogeniculate terminals in wild type and *math5*$^{-/-}$ mice contained no dendritic protrusions and dendrites postsynaptic to these terminals contained no detectable levels of GABA (Figure 2a–d; green).

In the Rbp4-cre line, cre-recombinase is expressed in most layer V cortical neurons, and a subset of layer VI cortical neurons (Adesnik, 2018; Grant et al., 2016; Gensat Brain Atlas, gensat.org). This line has been used to demonstrate changes in cortical innervation of the dLGN following perinatal monocular enucleation (Giasafaki et al., 2022; Grant et al., 2016).Therefore, we also labeled V1 corticogeniculate projections in Rbp4-cre mice and Rbp4-cre/*math5*$^{-/-}$ mice. We placed virus injections in V1 to induce the expression of peroxidase in a cre-dependent manner. These injections resulted in the labeling of a large number of layer V cortical neurons and a small number of layer VI neurons (Figure 4a,e). In the injected mice, we found that the majority of labeled profiles in the dLGN of both

Rbp4-cre mice and Rbp4-cre/*math5*$^{-/-}$ mice were myelinated axons that coursed through the dLGN (Figure 4b,f; Figure 5c,d). As previously described for monocularly enucleated mice (Grant et al., 2016), in the Rbp4-cre/*math5*$^{-/-}$ mice we found that many of these axons assumed a more dorsal position, occupying the region of the missing optic tract fibers (wild-type: Figure 4f arrow, 5a; *math5*$^{-/-}$: Figure 4d arrow; 5b). In the Rbp4-cre and Rbp4-cre/math5$^{-/-}$ mice, in addition to labeled myelinated axons, we were able to detect a small number labeled terminals that displayed RS morphology (Figure 5e; Rbp4-cre n= 10; Rbp4-cre/math5$^{-/-}$ n = 4) as well as unmyelinated axons that contained vesicles (Figure 5f).

Tectogeniculate terminals in WT, math5$^{-/-}$, Rpb4-cre, and Rpb4-cre/math5$^{-/-}$ mice

In the Rbp4-cre mouse line, cre-recombinase is also expressed in subsets of subcortical neurons, including areas such as the superior colliculus (SC; Grant et al., 2016; Gensat Brain Atlas, gensat.org) which projects to the shell region of the dLGN (Bickford et al., 2015). The presence of cre-recombinase in SC neurons in Rpb4-cre mice could explain why terminals are detected in the shell of the dLGN in Rpb4-cre mice crossed with reporter mice (Giasafaki et al., 2022; Grant et al., 2016). To test this, we labeled tectogeniculate projections in Rbp4-cre mice and Rbp4-cre/*math5*$^{-/-}$ mice by placing virus injections in the SC to induce the expression of fluorescent proteins in a cre-dependent or non-cre-dependent manner.

Cre-dependent virus injections in the SC of Rpb4-cre mice resulted in the labeling of subsets of neurons in the SC (Figure 4c) and sparse axons and boutons in the shell of the dLGN (Figure 4d, arrow). In Rbp4-cre/*math5*$^{-/-}$ mice, cre-dependent injections in the SC also labeled subsets of neurons in the SC (Figure 4g) and sparse axons and boutons in the shell of the dLGN (Figure 4h, arrow) which were similar in position and density to those labeled in Rpb4-cre mice. Moreover, non-cre-dependent virus injections placed in the SC of Rbp4-cre/*math5*$^{-/-}$ mice resulted in a band of labeled terminals confined to the shell of the dLGN (Figure 6b), as in wild-type animals (Figure 6a; Bickford et al., 2015).

These results indicate that the SC is one source of terminals labeled in the dLGN of Rbp4-cre mice crossed with reporter mice (Giasafaki et al., 2022; Grant et al., 2016). Tectogeniculate terminals are large “driver-like” terminals (Bickford et al., 2015) and therefore could account for some of the previously noted “retinogeniculate replacement terminals”. However, large terminals are not confined to the dLGN shell in *math5*$^{-/-}$ mice (El-Danaf et al., 2015), while we found that tectogeniculate terminals remain confined to the shell in *math5*$^{-/-}$ mice. Thus, additional sources of input likely contribute to the population of “retinogeniculate replacement terminals” observed in mice lacking retinal input.

Pedunculopontine tegmentum terminals in the dLGN of WT and math5$^{-/-}$ mice

Next, to examine the morphology and distribution of terminals that originate from the pedunculopontine tegmentum (PPT), we stained dLGN sections with antibodies against the vesicular acetylcholine transporter (VAChT), which we identified as a specific marker for this projection (Sokhadze et al., 2022). As illustrated in Figure 6 (c,d), in both wild type and math5$^{-/-}$ mice, the VAChT antibody labels diffusely distributed small puncta. Thus, the PPT is not a source of “retinogeniculate replacement terminals”.

Parabigeminal terminals in the dLGN of WT and math5$^{-/-}$ mice

Finally, we explored the parabigeminal nucleus (PBG) as a source of "retinogeniculate replacement terminals" since previous studies of Chat-cre and Chat-cre/*math5*$^{-/-}$ mice indicate significant plasticity in the PBG-dLGN projection (Sokhadze et al., 2018). As described in detail in Sokhadze et al. (2018), virus injections in the PBG of WT mice primarily label terminals in the contralateral dLGN, where they are most densely distributed in the shell; terminals in the ipsilateral dLGN are extremely sparse and confined to a small dorsomedial patch. However, in *math5*$^{-/-}$ mice the PBG projection expands and both the contralateral and ipsilateral dLGN are filled with a dense distribution of terminals.

At the ultrastructural level, in both wild type and *math5*$^{-/-}$mice, labeled PBG terminals engaged in synapses were generally large profiles that often contained dendritic protrusions (Figure 7a–c). Indeed, these terminals resembled the previously described "retinogeniculate replacement terminals" observed in anophthalmic, microphthalmic, enucleated, as well as *math5*$^{-/-}$ mice (Cullen & Kaiserman-Abramof, 1976; El-Danaf et al., 2015; Kaiserman-Abramof, 1983; Winkelmann et al., 1985). In fact, labeled PBG terminals in both C57Blk6 mice (Figure 7c, contralateral dLGN n = 321; 1.177±0.725 μm^2) and math5$^{-/-}$ mice (Figure 7a, ipsilateral dLGN n = 164; 1.812 ± 1.395 μm^2, Figure 7b, contralateral dLGN n = 153; 1.381 ± 0.893 μm^2) were found to be significantly larger than corticogeniculate terminals in wild type and *math5*$^{-/-}$ mice (Kruskal-Wallis, p<.0001).

As a population, PBG terminals were significantly smaller than retinogenicuate terminals (Figure 8; Kruskal-Wallis, p <.0001). However, there was considerable overlap in the sizes of these terminal populations, with many PBG terminal profiles reaching the size of the largest retinogeniculate terminal profiles and/or exceeding the size of the smaller retinogeniculate terminal profiles. This was especially evident for PBG terminals in *math5*$^{-/-}$ mice (Figure 9, ipsilateral and contralateral measurements combined). In addition, a large proportion of PBG terminals in both wild type (35.8%) and math5−/− (55.5%) mice contained dendritic protrusions.

Although there was no significant difference in the sizes of contralateral PBG terminals in the dLGN of wild type versus *math5*$^{-/-}$ mice (Figure 10; Kruskal-dWallis, p=.1270), ipsilateral PBG terminals in the dLGN of *math5*$^{-/-}$ mice were found to be significantly larger than contralateral PBG terminals in the dLGN of wild type mice (Figure 10; Kruskal-Wallis, p < 0.0001).

Discussion

To identify the source of "retinogeniculate replacement terminals", we compared all sources of nonGABAergic input to the dLGN in mice with and without retinofugal input. While previous reports have suggested that layer V cortical neurons provide an anomolous source of input following monocular or binocular enucleation (Frangeul et al., 2016; Giasafaki et al., 2022; Grant et al., 2016), we found no differences in the ultrastructure of corticogeniculate terminals in wild type versus *math5*$^{-/-}$ mice. We also found no changes in overall pattern of tectogeniculate or PPT projections in wild type versus *math5*$^{-/-}$ mice. In contrast, terminals that originate from the PBG expand their innervation territory in the

dLGN of *math5*$^{-/-}$ mice (Sokhadze et al., 2018) and these terminals exhibit characteristics of retinal terminals in both wild type and *math5*$^{-/-}$ mice; i.e. synapses on dendrites that protrude into large terminals filled with round synaptic vesicles and multiple mitochondria. We conclude that projections from the PBG expand to fill the vacancies left by the lack of retinal ganglion cell input in the dLGN of math5$^{-/-}$ mice and are the likely source of "retinogeniculate replacement terminals" previously observed in this mouse line (El-Danaf et al, 2015).

Corticogeniculate input in the absence of retinogeniculate input

Previous studies in *math5*$^{-/-}$ mice have indicated that the lack of retinogeniculate input results in changes in the timing of corticogeniculate innervation (Brooks et al., 2013; Seabrook et al., 2013). Normally, corticogeniculate axons begin to innervate the dLGN at P3 and complete their innervation by the second postnatal week, the time of natural eye opening. However, in *math5*$^{-/-}$ mice, corticogeniculate innervation is accelerated, beginning at P0, with completion by the end of the first postnatal week. This effect has been shown to be regulated by the expression of the chondroitin sulfate proteoglycan (CSPG), aggrecan. Aggrecan, a repulsive CSPG, is transiently expressed in the developing dLGN, showing enriched levels at early postnal ages, and inhibiting cortical axons from prematurely entering. Postnatal loss of aggrecan from dLGN coincides with upregulation of aggrecanase expression and the age-related progression of corticogeniculate innervation. However, in the absence of retinal input aggrecan expression is low and aggreganases high, allowing for the accelerated innervation of corticogeniculate input.

Here we found that the change in the timing of corticogeniculate innervation in *math5*$^{-/-}$ mice does not result in any differences in the ultrastruture of corticogeniculate synapses, since we found no difference in the sizes of corticogeniculate teminals in wild-type versus *math5*$^{-/-}$ mice. Moreover, the only changes we observed in V1 projections labeled in a cre-dependent manner in RpB4-cre and Rpb4-cre/*math5*$^{-/-}$ mice was the change in the position of axons that course through the dLGN en route to other targets.

These results seem at odds with previous studies using RpB4-cre mice crossed with reporter lines to demonstrate changes in cortical innervation patterns following monocular enucleation (Giasafaki et al., 2022; Grant et al., 2016). Although a subset of tectogeniculate cells contain cre-recombinase in the Rpb4-cre line, we found no apparent expansion of tectogeniculate projections in *math5*$^{-/-}$ mice. Moreover, cre-dependent virus injections in V1 of RpB4-cre mice that received monocular or binocular enucleation have demonstrated changes in both V1 innervation of the dLGN and activation of dLGN neurons (Frangeul et al., 2016; Giasafaki et al., 2022; Grant et al., 2016). Thus, these discrepancies may pertain to the use of early postnatal enucleation versus the use of *math5*$^{-/-}$ mice as a means to achieve a genetic form of deafferentation. This suggests that changes in corticogeniculate innervation are not induced by the lack of retinal input per se, but may be caused by other mitigating factors. Indeed, inflammation brought about by retinal degeneration and/or the disruption of genes associated with axon guidance, neuronal migration, and synaptogenesis (Frangeul et al., 2016; Giasafaki et al., 2022) could produce changes in corticogeniculate innervation patterns that are not detected in *math5*$^{-/-}$ mice.

Comparison of synaptic terminals that originate from the retina and the PBG

Besides their size and comparable synaptic arrangements, there are additional similarities between synaptic terminals that originate from the retina and the PBG. First, both projections are bilateral and enter the dLGN via the optic tract. In mice with intact retinofugal projections, the contralateral PBG projection reaches the dLGN via axons that travel rostrally, cross to the contralateral side in the supraoptic decussation, and enter the dLGN via the optic tract (Sokhadze et al., 2018; Watanabe & Kawana, 1979). The ipsilateral PBG projection similarly travels in the optic tract to innervate a small dorsomedial region of the dLGN. Therefore, although the ipsilateral projection from the PBG to the dLGN is normally quite restricted, pathways to access both the ipsilateral and contralateral dLGN are normally present in wild type mice. In *math5*$^{-/-}$ mice, the PBG axons follow a similar trajectory to cross the midline in the supraoptic decussation, but in the absence of an optic tract they traverse the thalamus to target the dLGN (Sokhadze et al., 2018).

PBG and retinal projections are also similar in that both PBG cells and retinal ganglion cells express the type 2 glutamate transporter (vGLUT2; Steinkellner et al., 2019). Therefore, like retinal terminals, PBG terminals probably release glutamate from the abundant round synaptic vesicles contained within them. PBG innervation may account for at least some of the vGLUT2-positive puncta in the dLGN that remain in *math5*$^{-/-}$ and enucleated mice (Bhandari et al., 2022; El-Danaf et al., 2015). PBG cells also express choline acetyl transferase (ChAT), but do not express the vesicular acetylcholine transporter (VAChT; Sokhadze et al., 2022). Similarly, VAChT mRNA is undetectable in a subdivision of the avian PBG homologue (nucleus isthmi parvocellularis) where ChAT mRNA is colocalized with vGLUT2 mRNA (González-Cabrera et al., 2015). Therefore, it is unclear whether PBG terminals co-release glutamate and acetylcholine.

Interestingly, we found no evidence for plasticity in other brainstem projections. Tectogeniculate projections normally form large “driver-like” terminals that converge with retinal terminals to innervate single neurons in the shell of the ipsilateral dLGN (Bickford et al., 2015). In *math5*$^{-/-}$ mice, tectogeniculate terminals remain confined to the dorsal and lateral regions of the ipsilateral dLGN and do not appear to expand their innervation territory to the dLGN core or the contralateral dLGN. Likewise, we found no differences in PPT projections labeled using immunocytochemistry in wild type and *math5*$^{-/-}$ mice. Thus, the plasticity of the PBG-dLGN projection appears to be unique.

Implications for retinal reinnervation of the dLGN

The mechanisms underlying the expansion of the PBG pathway are of potential interest for studies interrogating potential treatments for diseases or trauma that result in retinal degeneration. “Retinal replacement terminals” have been identified in mice enucleated as late as 20 days after birth (Cullen & Kaiserman-Abramof, 1976). Therefore, strategies to regenerate retinal innervation of the dLGN should consider potential competition from remodeled synaptic circuits. On the other hand, it is unknown whether “retinal replacement terminals” are present in other species. In most species, the PBG projections are segregated in discrete regions of dLGN (e.g., C-laminae of carnivores, koniocellular layers of primates;

Harting et al., 1991), and it is unclear whether these terminals can expand into other areas of the dLGN following the loss of retnal input.

Implications regarding cross modal plasticity

The function of the expanded PBG-dLGN projection in the absence of retinal input is currently unclear. Normally, the PBG receives all of its input from the visual layers of the superior colliculus (Deichler et al., 2020; Shang et al., 2015; Whyland et al., 2020), and PBG neurons respond to moving visual stimuli(Cui & Malpeli, 2003; Ma et al., 2013; Reinhard et al., 2019). In the absence of retinal input, the superior colliculus could potentially transmit auditory or somatosensory signals to the PBG which could be relayed to the dLGN (Basso et al., 2021; Stevenson & Lund, 1982). The dLGN could then relay these other sensory modalities to the cortex. The transmission of anomalous inputs to the visual cortex in the absence of retinal input has been noted in several previous studies (Izraeli et al., 2002; Kahn & Krubitzer, 2002; Piché et al., 2007; Yaka et al., 2000), and the identification of the PBG as a source of “retinal replacement terminals” in the dLGN suggests that subcortical pathways may be involved in this transfer of nonvisual sensory signals to the visual cortex.

Acknowledgments

This work was supported by the National Eye Institute grants T35EY026509, R01EY031322, and F31EY030746 and the National Insittue of General Medical Sciences grant P20GM103436.

Data Availability Statement:

The data that support the findings of this study are available from the corresponding author upon reasonable request.

References cited:

Abbott CW, Kozanian OO, & Huffman KJ (2015). The effects of lifelong blindness on murine neuroanatomy and gene expression. Frontiers in Aging Neuroscience, 7(JUL). 10.3389/fnagi.2015.00144

Adesnik H (2018). Layer-specific excitation/inhibition balances during neuronal synchronization in the visual cortex. Journal of Physiology, 596(9), 1639–1657. 10.1113/JP274986 [PubMed: 29313982]

Augustinaite S, & Kuhn B (2020). Complementary Ca2+ Activity of Sensory Activated and Suppressed Layer 6 Corticothalamic Neurons Reflects Behavioral State. Current Biology, 30(20), 3945–3960.e5. 10.1016/j.cub.2020.07.069 [PubMed: 32822605]

Basso MA, Bickford ME, & Cang J (2021). Unraveling circuits of visual perception and cognition through the superior colliculus. In Neuron (Vol. 109, Issue 6, pp. 918–937). Cell Press. 10.1016/j.neuron.2021.01.013 [PubMed: 33548173]

Bhandari A, Ward TW, Smith J, & van Hook MJ (2022). Structural and Functional Plasticity in the Dorsolateral Geniculate Nucleus of Mice following Bilateral Enucleation. Neuroscience, 488, 44–59. 10.1016/j.neuroscience.2022.01.029 [PubMed: 35131394]

Bickford ME, Slusarczyk A, Dilger EK, Krahe TE, Kucuk C, & Guido W (2010). Synaptic development of the mouse dorsal lateral geniculate nucleus. Journal of Comparative Neurology, 518(5), 622–635. 10.1002/cne.22223 [PubMed: 20034053]

Bickford ME, Zhou N, Krahe TE, Govindaiah G, & Guido W (2015). Retinal and tectal “Driver-Like” inputs converge in the shell of the mouse dorsal lateral geniculate nucleus. Journal of Neuroscience, 35(29), 10523–10534. 10.1523/JNEUROSCI.3375-14.2015 [PubMed: 26203147]

Brooks JM, Su J, Levy C, Wang JS, Seabrook TA, Guido W, & Fox MA (2013). A molecular mechanism regulating the timing of corticogeniculate innervation. Cell Reports, 5(3), 573–581. 10.1016/j.celrep.2013.09.041 [PubMed: 24183669]

Charalambakis NE, Govindaiah G, Campbell PW, & Guido W (2019). Developmental remodeling of thalamic interneurons requires retinal signaling. Journal of Neuroscience, 39(20), 3856–3866. 10.1523/JNEUROSCI.2224-18.2019 [PubMed: 30842249]

Cui H, & Malpeli JG (2003). Activity in the parabigeminal nucleus during eye movements directed at moving and stationary targets. Journal of Neurophysiology, 89(6), 3128–3142. 10.1152/jn.01067.2002 [PubMed: 12611992]

Cullen MJ, & Kaiserman-Abramof IR (1976). Cytological organization of the dorsal lateral geniculate nuclei in mutant anophthalmic and postnatally enucleated mice. Journal of Neurocytology, 5(4), 407–424. 10.1007/BF01181648 [PubMed: 993820]

Deichler A, Carrasco D, Lopez-Jury L, Vega-Zuniga T, Márquez N, Mpodozis J, & Marín GJ (2020). A specialized reciprocal connectivity suggests a link between the mechanisms by which the superior colliculus and parabigeminal nucleus produce defensive behaviors in rodents. Scientific Reports, 10(1). 10.1038/s41598-020-72848-0

El-Danaf RN, Krahe TE, Dilger EK, Bickford ME, Fox MA, & Guido W (2015). Developmental remodeling of relay cells in the dorsal lateral geniculate nucleus in the absence of retinal input. Neural Development, 10(1), 19. 10.1186/s13064-015-0046-6 [PubMed: 26174426]

Fitzpatrick D, Penny GR, & Schmechel ADE (1984). Glutamic Acid Decarboxylase-Immunoreactive Neruons and Terminals in the Lateral Geniculate Nucleus of the Cat (Vol. 4, Issue 7).

Frangeul L, Pouchelon G, Telley L, Lefort S, Luscher C, & Jabaudon D (2016). A cross-modal genetic framework for the development and plasticity of sensory pathways. Nature, 538(7623), 96–98. 10.1038/nature19770 [PubMed: 27669022]

Giasafaki C, Grant E, Hoerder-Suabedissen A, Hayashi S, Lee S, & Molnár Z (2022). Cross-hierarchical plasticity of corticofugal projections to dLGN after neonatal monocular enucleation. Journal of Comparative Neurology, 530(7), 978–997. 10.1002/cne.25304 [PubMed: 35078267]

Goldberg JL, Guido W, Anderson A, Benowitz L, Benson D, Bharti K, Blumenkranz M, Smead HJ, Brooks B, Constantine-Paton M, Crair M, Diamond J, Dowling J, Fawcett J, Feldheim D, Frishman L, Goldberg J, Goldman D, Guido W, … Zhou F (2016). Report on the national eye institute audacious goals initiative: Regenerating the optic nerve. Investigative Ophthalmology and Visual Science, 57(3), 1201–1205. 10.1167/iovs.15-18500 [PubMed: 26978025]

González-Cabrera C, Garrido-Charad F, Roth A, & Marín GJ (2015). The isthmic nuclei providing parallel feedback connections to the avian tectum have different neurochemical identities: Expression of glutamatergic and cholinergic markers in the chick (Gallus gallus). Journal of Comparative Neurology, 523(9), 1341–1358. 10.1002/cne.23739 [PubMed: 25594665]

Grant E, Hoerder-Suabedissen A, & Molnár Z (2016). The Regulation of Corticofugal Fiber Targeting by Retinal Inputs. Cerebral Cortex, 26(3), 1336–1348. 10.1093/cercor/bhv315 [PubMed: 26744542]

Gupta N, Greenberg G, de Tilly LN, Gray B, Polemidiotis M, & Yücel YH (2009). Atrophy of the lateral geniculate nucleus in human glaucoma detected by magnetic resonance imaging. British Journal of Ophthalmology, 93(1), 56–60. 10.1136/bjo.2008.138172 [PubMed: 18697810]

Hammer S, Monavarfeshani A, Lemon T, Su J, & Fox MA (2015). Multiple Retinal Axons Converge onto Relay Cells in the Adult Mouse Thalamus. Cell Reports, 12(10), 1575–1583. 10.1016/j.celrep.2015.08.003 [PubMed: 26321636]

Harting JK, Huerta MF, Hashikawa T, & Van DP (1991). Projection of the Mammalian Superior Colliculus Upon the Dorsal Lateral Geniculate Nucleus: Organization of Tectogeniculate Pathways in Nineteen Species. In THE JOURNAL OF COMPARATIVE NEUROLOGY (Vol. 304).

Houser CR, Vaughn JE, Barber RP, & Roberts E (1980). GABA neurons are the major cell type of the nucleus reticularis thalami. Brain Research, 200(2), 341–354. 10.1016/0006-8993(80)90925-7 [PubMed: 7417821]

Izraeli R, Koay G, Lamish M, Heicklen-Klein AJ, Heffner HE, Heffner RS, & Wollberg Z (2002). Cross-modal neuroplasticity in neonatally enucleated hamsters: structure, electrophysiology and

behaviour. European Journal of Neuroscience, 15(4), 693–712. 10.1046/j.1460-9568.2002.01902.x [PubMed: 11886450]

Kahn DM, & Krubitzer L (n.d.). Massive cross-modal cortical plasticity and the emergence of a new cortical area in developmentally blind mammals. www.pnas.orgcgidoi10.1073pnas.162342799

Kaiserman-Abramof IR (1983). Intrauterine enucleation of normal mice mimics a structural compensatory response in the geniculate of eyeless mutant mice. Brain Research, 270(1), 149–153. 10.1016/0006-8993(83)90804-1 [PubMed: 6871708]

Ma R, Cui H, Lee S-H, Anastasio TJ, & Malpeli JG (2013). Predictive encoding of moving target trajectory by neurons in the parabigeminal nucleus. J Neurophysiol, 109, 2029–2043. 10.1152/jn.01032.2012.-Intercepting [PubMed: 23365185]

Montera VM, & Zempel J (1985). Evidence for two types of GABA-containing interneurons in the A-laminae of the cat lateral geniculate nucleus: a double-label HRP and GABA-immunocytochemical study. Experimental Brain Research, 60(3), 603–609. 10.1007/BF00236949 [PubMed: 2416585]

Montero VM, & Singer W (1984). Ultrastructure and synaptic relations of neural elements containing glutamic acid decarboxylase (GAD) in the perigeniculate nucleus of the cat - A light and electron microscopic immunocytochemical study. Experimental Brain Research, 56(1), 115–125. 10.1007/BF00237447 [PubMed: 6381084]

Morgan JL, & Lichtman JW (2020). An Individual Interneuron Participates in Many Kinds of Inhibition and Innervates Much of the Mouse Visual Thalamus. Neuron, 106(3), 468–481.e2. 10.1016/j.neuron.2020.02.001 [PubMed: 32142646]

Piché M, Chabot N, Bronchti G, Miceli D, Lepore F, & Guillemot JP (2007). Auditory responses in the visual cortex of neonatally enucleated rats. Neuroscience, 145(3), 1144–1156. 10.1016/j.neuroscience.2006.12.050 [PubMed: 17276013]

Ptito M, Paré S, Dricot L, Cavaliere C, Tomaiuolo F, & Kupers R (2021). A quantitative analysis of the retinofugal projections in congenital and late-onset blindness. NeuroImage: Clinical, 32, 102809. 10.1016/j.nicl.2021.102809 [PubMed: 34509923]

Reinhard K, Li C, Do Q, Burke EG, Heynderickx S, & Farrow K (2019). A projection specific logic to sampling visual inputs in mouse superior colliculus. ELife, 8. 10.7554/eLife.50697

Seabrook TA, El-Danaf RN, Krahe TE, Fox MA, & Guido W (2013). Retinal input regulates the timing of corticogeniculate innervation. Journal of Neuroscience, 33(24), 10085–10097. 10.1523/JNEUROSCI.5271-12.2013 [PubMed: 23761904]

Shang C, Liu Z, Chen Z, Shi Y, Wang Q, Liu S, Li D, & Cao P (2015). A parvalbumin-positive excitatory visual pathway to trigger fear responses in mice. Science, 348(6242), 1472–1477. 10.1126/science.aaa8694 [PubMed: 26113723]

Sokhadze G, Seabrook TA, & Guido W (2018). The absence of retinal input disrupts the development of cholinergic brainstem projections in the mouse dorsal lateral geniculate nucleus 11 Medical and Health Sciences 1109 Neurosciences. Neural Development, 13(1). 10.1186/s13064-018-0124-7

Sokhadze G, Whyland KL, Bickford ME, & Guido W (2022). The organization of cholinergic projections in the visual thalamus of the mouse. Journal of Comparative Neurology, 530(7), 1081–1098. 10.1002/cne.25235 [PubMed: 34448209]

Steinkellner T, Yoo JH, & Hnasko TS (2019). Differential expression of VGLUT2 in mouse mesopontine cholinergic neurons. ENeuro, 6(4). 10.1523/ENEURO.0161-19.2019

Stevenson JA, & Lund RD (1982). A crossed parabigemino-lateral geniculate projection in rats blinded at birth. Experimental Brain Research, 45(1–2), 95–100. 10.1007/BF00235767 [PubMed: 6173253]

Wang SW, Kim BS, Ding K, Wang H, Sun D, Johnson RL, Klein WH, & Gan L (2001). Requirement for math5 in the development of retinal ganglion cells. Genes and Development, 15(1), 24–29. 10.1101/gad.855301 [PubMed: 11156601]

Watanabe K, & Kawana E (1979). Efferent projections of the parabigeminal nucleus in rats: A horseradish peroxidase (HRP) study. Brain Research, 168(1), 1–11. 10.1016/0006-8993(79)90123-9 [PubMed: 455073]

Whyland KL, Slusarczyk AS, & Bickford ME (2020). GABAergic cell types in the superficial layers of the mouse superior colliculus. Journal of Comparative Neurology, 528(2), 308–320. 10.1002/cne.24754 [PubMed: 31396959]

Winkelmann E, Garey LJ, & Brauer K (1985). Ultrastructural development of the dorsal lateral geniculate nucleus of genetically microphthalmic mice. Experimental Brain Research, 60(3), 527–534. 10.1007/BF00236938 [PubMed: 4076375]

Yaka R, Yinon U, Rosner M, & Wollberg Z (2000). Pathological and experimentally induced blindness induces auditory activity in the cat primary visual cortex. Experimental Brain Research, 131(1), 144–148. 10.1007/s002219900295 [PubMed: 10759180]

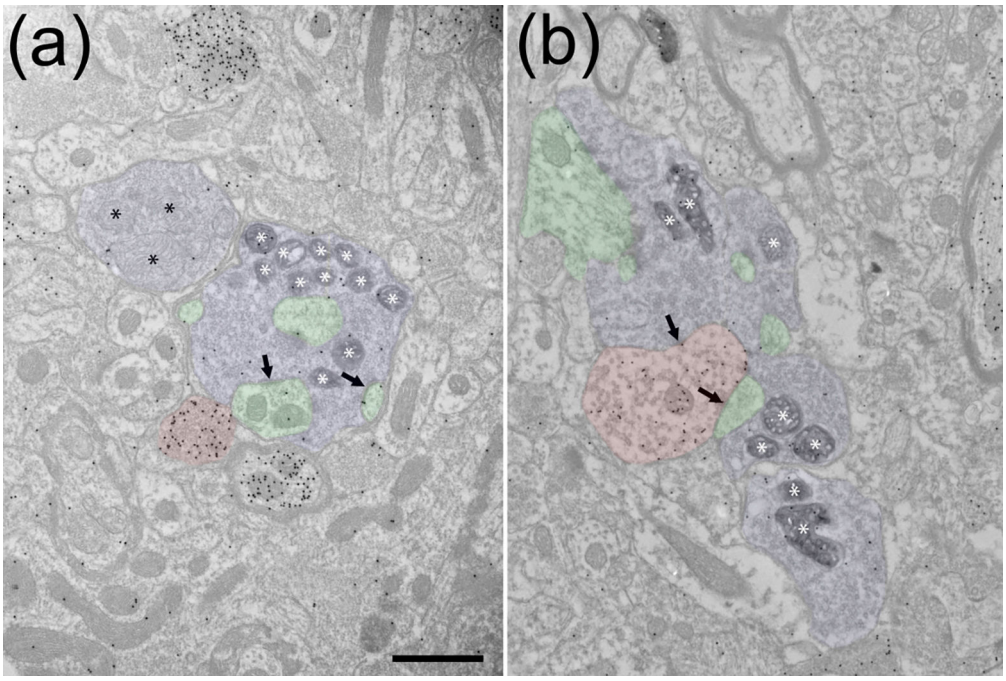

Figure 1: Retinogeniculate terminals in WT mice.

Electron micrographs illustrate ipsilateral (a) and contralateral (b) retinogeniculate terminals (blue overlay) labeled via monocular virus injections in C57Blk6 mice that induced the expression of peroxidase in mitochondria (white asterisks). The tissue was stained to detect GABA with gold particles. Unlabeled retinogeniculate terminals contain pale mitochondria (black asterisks, a). Retinogeniculate terminals both contain and synapse (black arrows) on the dendrites of nonGABAergic thalamocortical cells (a, green overlay, identified by a low density of gold particles) that often protrude into the terminals. Retinogeniculate terminals also contact the dendritic terminals of GABAergic interneurons (b, F2 profiles, red overlay, GABA content identified by a high density of overlying gold particles). The illustrated F2 profile synapses (black arrow) on a thalamocortical cell dendrite (green overlay, identified by a low density of overlying gold particles). Scale bar = 1 μm and applies to both panels.

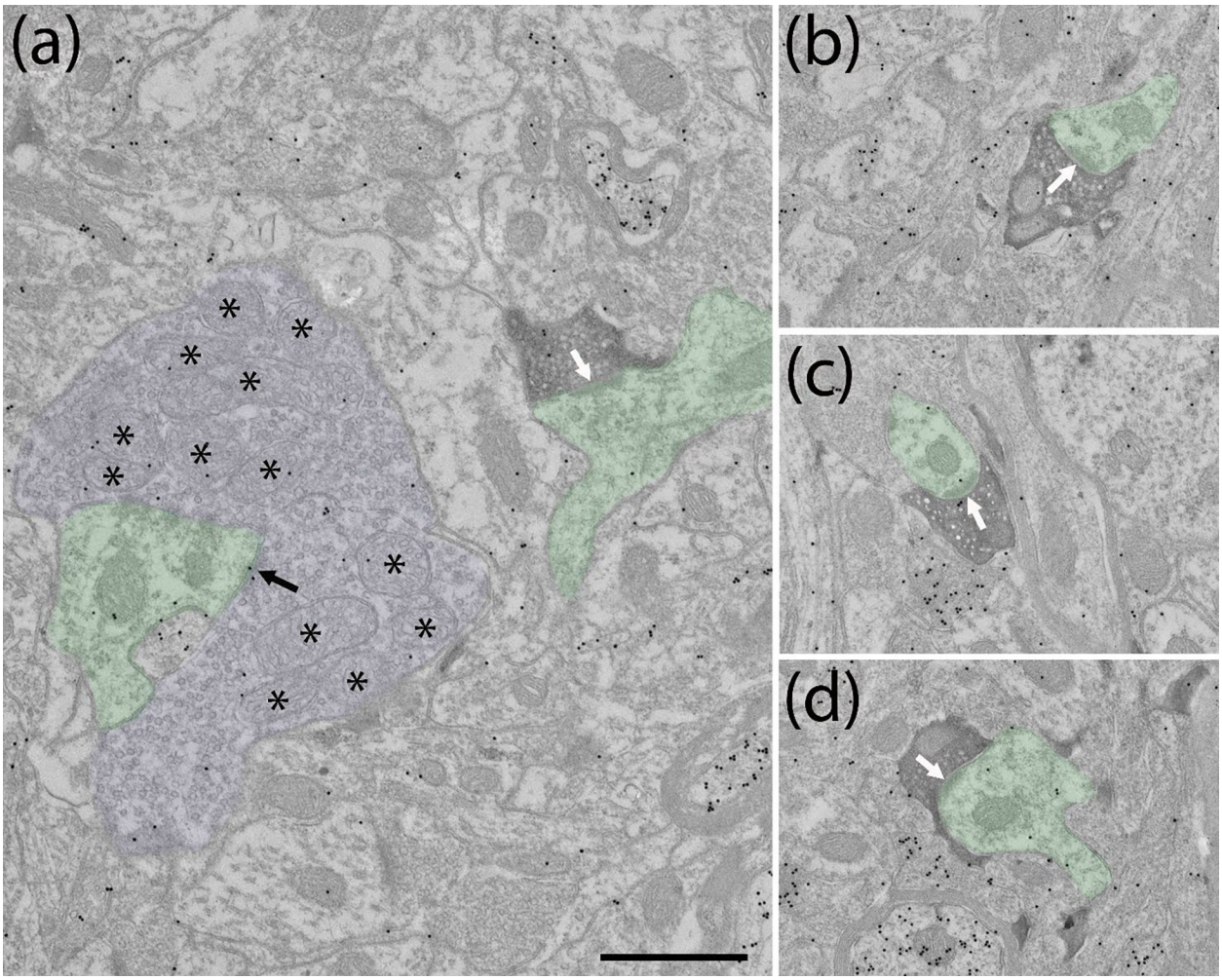

Figure 2: Corticogeniculate terminals in WT and *math5*$^{-/-}$ mice.

Electron micrographs illustrate corticogeniculate terminals labeled via V1 BDA injections in C57Blk6 (a) and *math5*$^{-/-}$ (b-d) mice. The tissue was stained to detect GABA with gold particles. In both WT and *math5*$^{-/-}$ mice, V1 terminals are small profiles that contain round synaptic vesicles (RS profiles) that synapse (white arrows) on thalamocortical cell dendrites (green overlay, low density of gold particles). In the electron micrograph illustrating the WT corticogeniculate terminal, an adjacent unlabeled retinal terminal (blue overaly, identified by its pale mitochondria, black asterisks) also contacts (black arrow) a thalamocortical cell dendrite (green overlay). Scale bar = 800nm and applies to all panels.

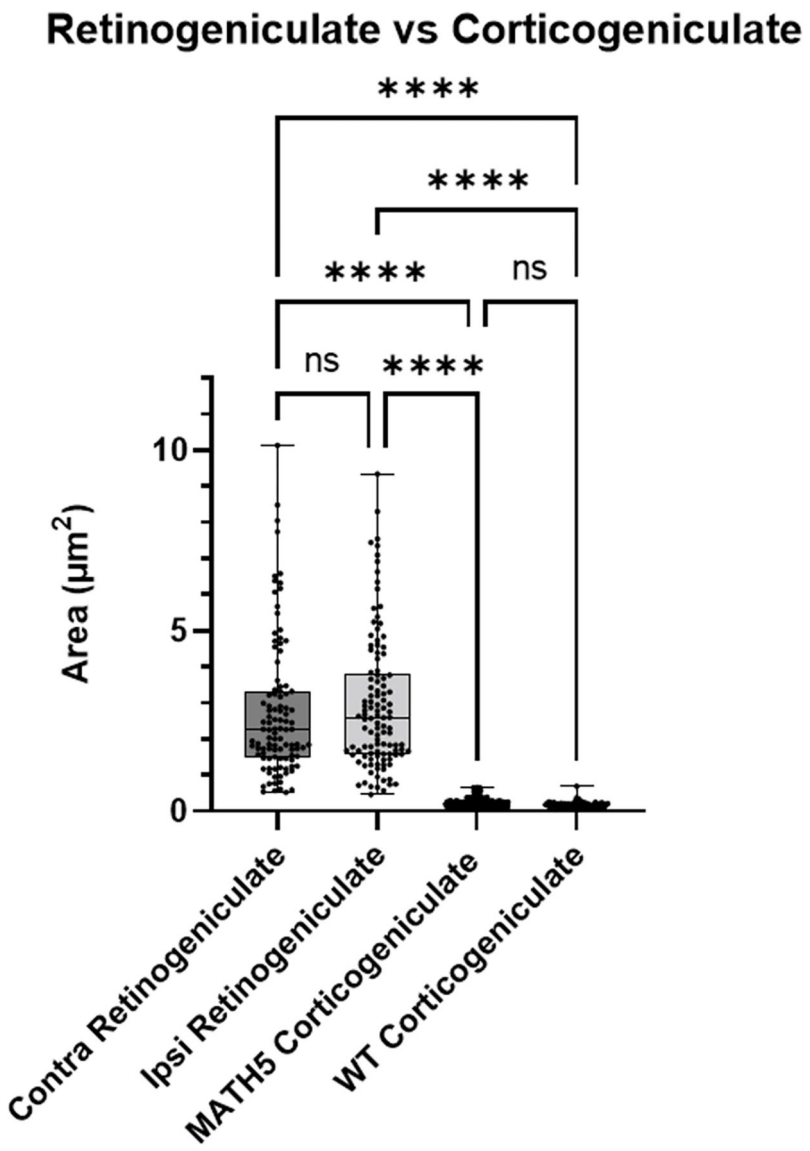

Figure 3:

Retinogeniculate terminals in C57Blk6 (WT) mice are significantly larger than corticogeniculate terminals in WT mice and *math5*$^{-/-}$ mice (**** $p < 0.0001$). There is no significant difference in the size of ipsilateral and contralateral retinogeniculate terminals in WT mice and no significant difference in the sizes of corticogeniculate terminals in WT and math5−/− mice (ns).

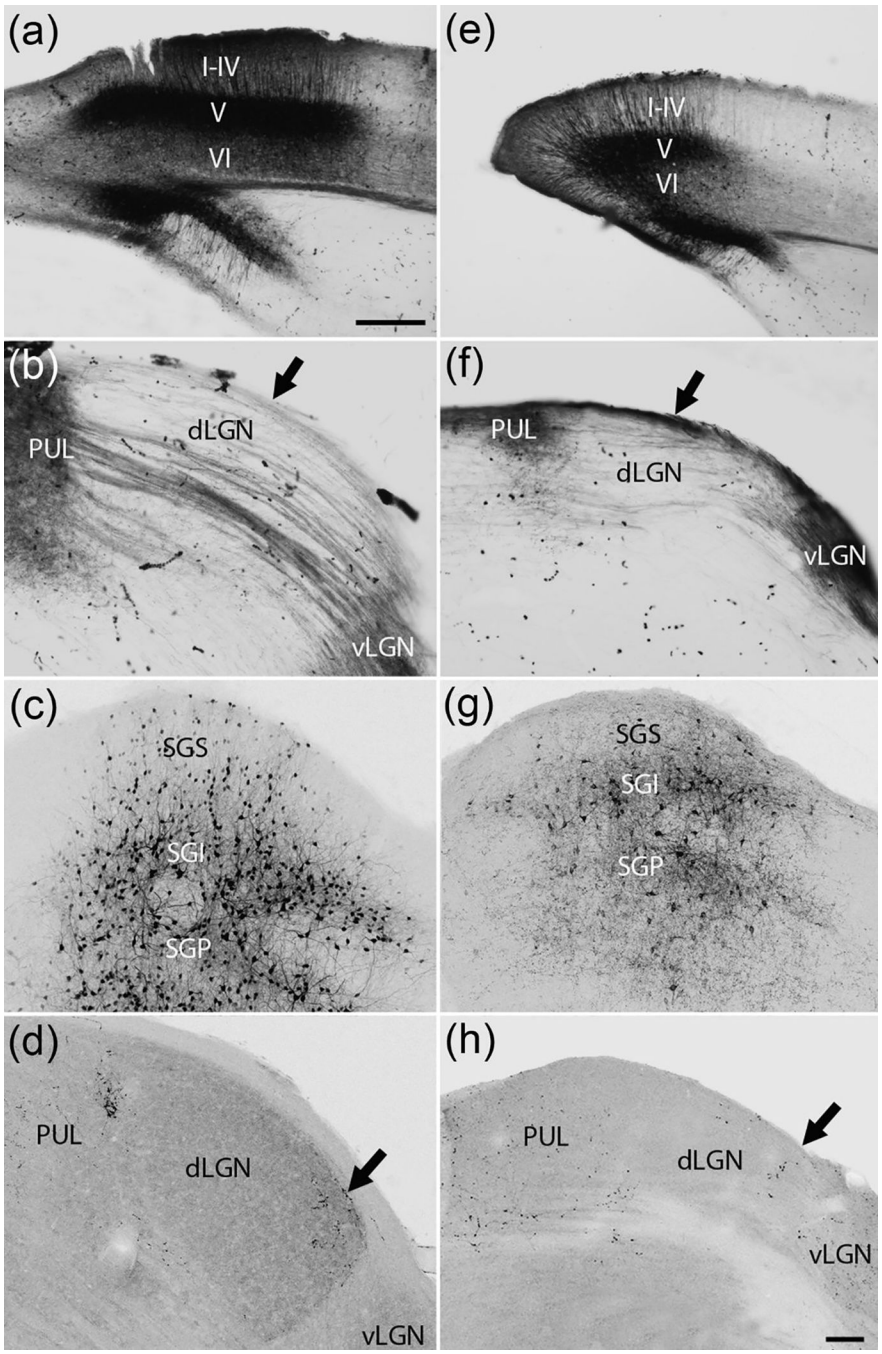

Figure 4: Cre-dependent V1 and SC projections to the dLGN of Rpb4-cre and Rpb4-cre/ *math5*$^{-/-}$ mice.

Cre-dependent (cell-filling) virus injections in V1 in Rpb4-cre (a,b) and Rpb4-cre/ *math5*$^{-/-}$ mice (e,f) labeled a dense population of cells in layer V that extended dendrites into layers I-IV, a smaller population of cells in layer VI, dense population of terminals in the ipsilateral pulvinar (PUL) and ventral lateral geniculate nucleus (vLGN), and axons that course through the ipsilateral dorsal lateral geniculate nucleus (dLGN). In Rpb4-cre mice, most labeled axons avoid the optic tract (b, arrow). In Rbb4-cre/ *math5*$^{-/-}$ mice, the position of many of the labeled axons shifted dorsally to occupy the position of the missing optic

tract (f, arrow). Cre-dependent (cell-filling) virus injections in the SC of Rpb4-cre (c,d) and Rbb4-cre/*math5*$^{-/-}$ mice (g,h) labeled subpopulation of cells in the stratum griseum superficiale (SGS), stratum griseum intermediale (SGI) and stratum griseum profundum (SGP) and a sparse population of terminals in the ipsilateral dorsolateral shell of the dLGN (d,h arrows). Scale in a = 500 μm and also applies to e. Scale in h = 100 μm and also applies to b-d and f-g.

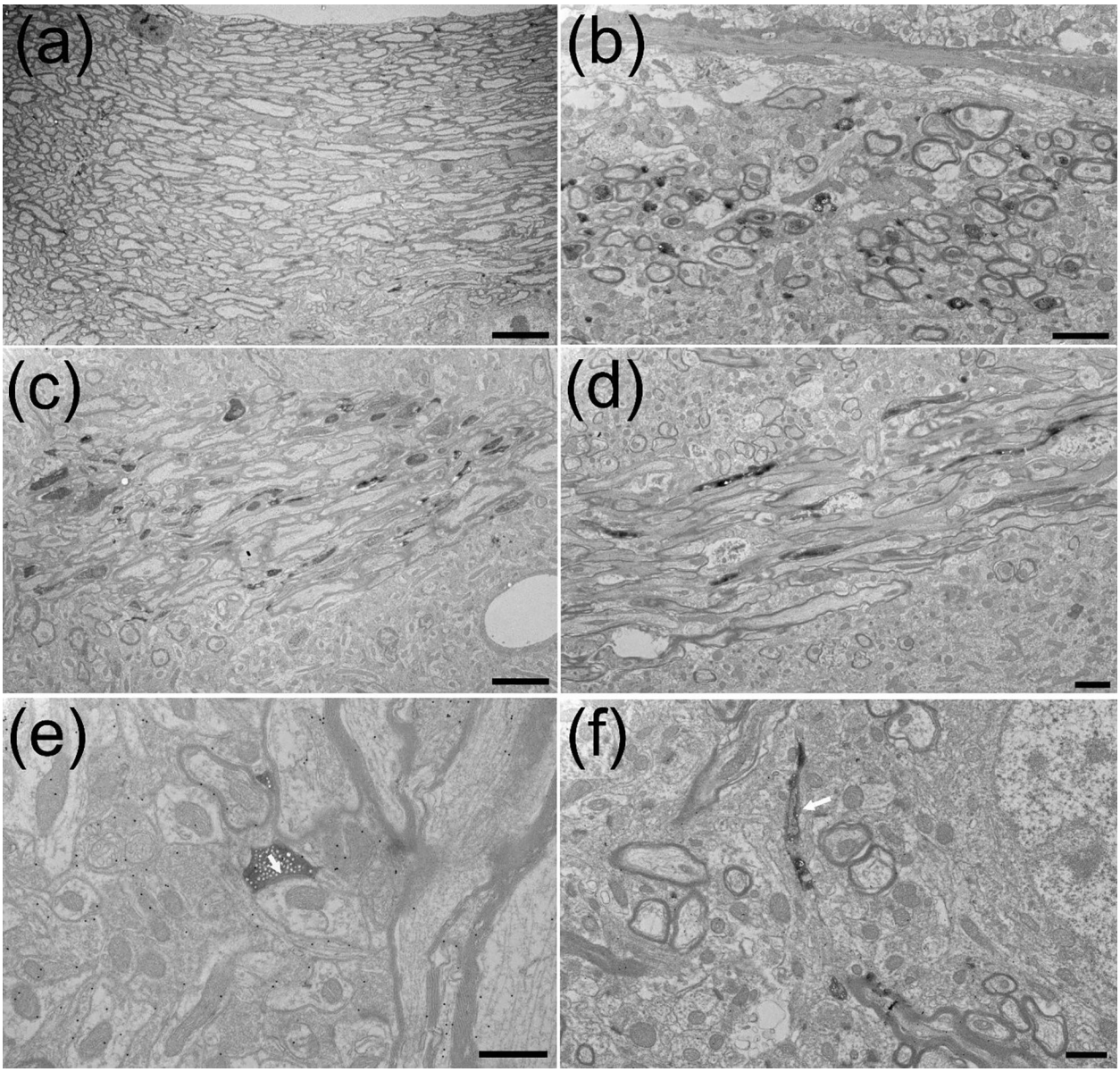

Figure 5:

Electron micrographs illustrate the ultrastructure of the dLGN in Rpb4-cre mice (a,c,e) and Rpb4-cre/Math5−/− mice (b,d,f) that received cre-dependent (cell-filling) virus injections in the ipsilateral V1. In Rpb4-cre mice, the optic tract at the dorsal surface of the dLGN is a thick layer of unlabeled myelinated axons (a). In Rpb4/math5−/− mice, the dorsal surface of the dLGN contains labeled axons in the location of the missing optic tract (b). Labeled axons course through the body of the dLGN in both Rpb4-cre (c) and Rpb4/math5−/− (d) mice. In both Rpb4-cre and Rpb4-cre/math5−/− mice, sparse labeled terminals that displayed RS morphology (e, white arrow indicates synapse, RPb4-cre) and unmyelinated fibers that contained vesicles (f, white arrow Rpb4-cre/math5−/−) were occasionally observed. Scale bars: a = 8 μm, b= 2 μm, c = 4 μm, d = 2 μm, e = 800 nm, f = 1 μm.

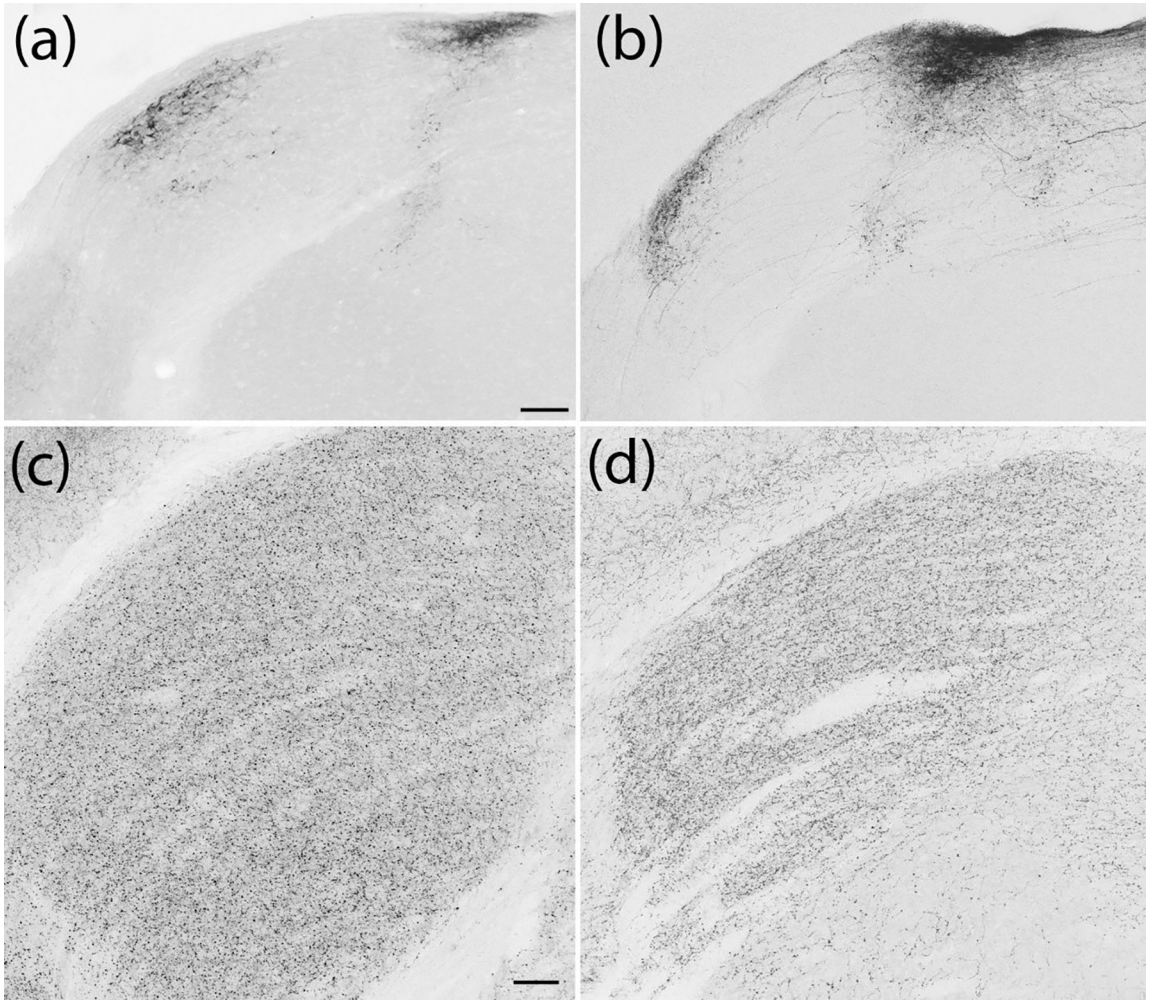

Figure 6: SC and PPT projections to the dLGN of WT and *math5*$^{-/-}$ mice.

Tectogeniculate projections labeled via virus injections in the ipsilateral SC innervate the dorsolateral shell of the dLGN in WT (a; from Bickford et al. 2015) and *math5*$^{-/-}$ mice (b). An antibody against the vesicular acetylcholine transporter labels small diffusely distributed terminals in both WT (c; from Sokhadze et al. 2022) and *math5*$^{-/-}$ mice (d). Scale in a = 100 μm and also applies to b. Scale in c = 50 μm and also applies to d.

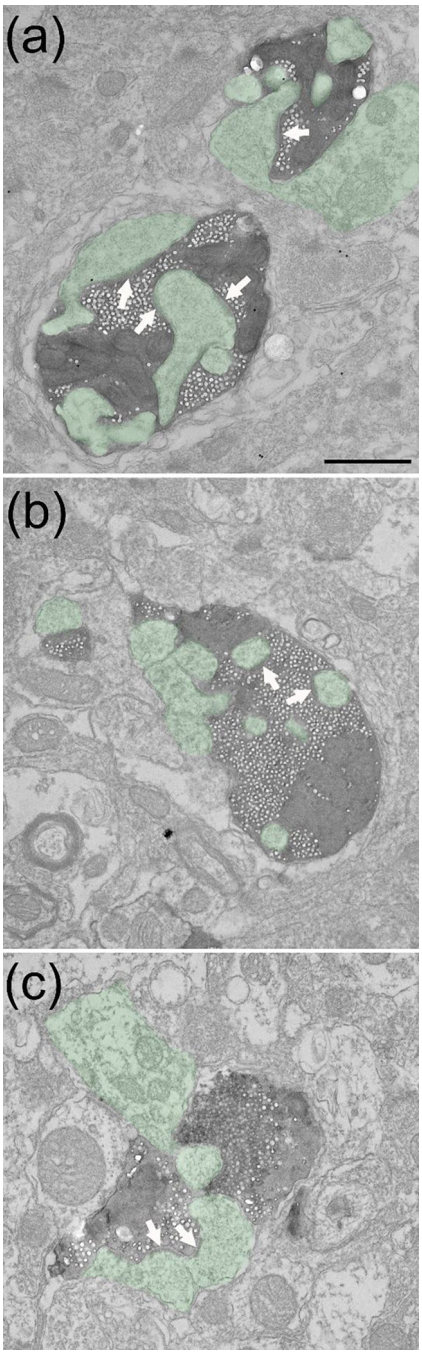

Figure 7: PBG terminals in the dLGN of WT and *math5*$^{-/-}$ mice.

Electron micrographs illustrate the ulstrastructure of dLGN terminals labeled via unilateral PBG (cell-filling) virus injections in *math5*$^{-/-}$ (a, ipsilateral dLGN c, contralateral dLGN) and C57Blk6 mice (c, contralateral dLGN). PBG terminals in the dLGN are large profiles that often contain and synapse (white arrows) on dendrites (green overlay) that protrude into the labeled terminals. Scale bar = 800nm and applies to all panels.

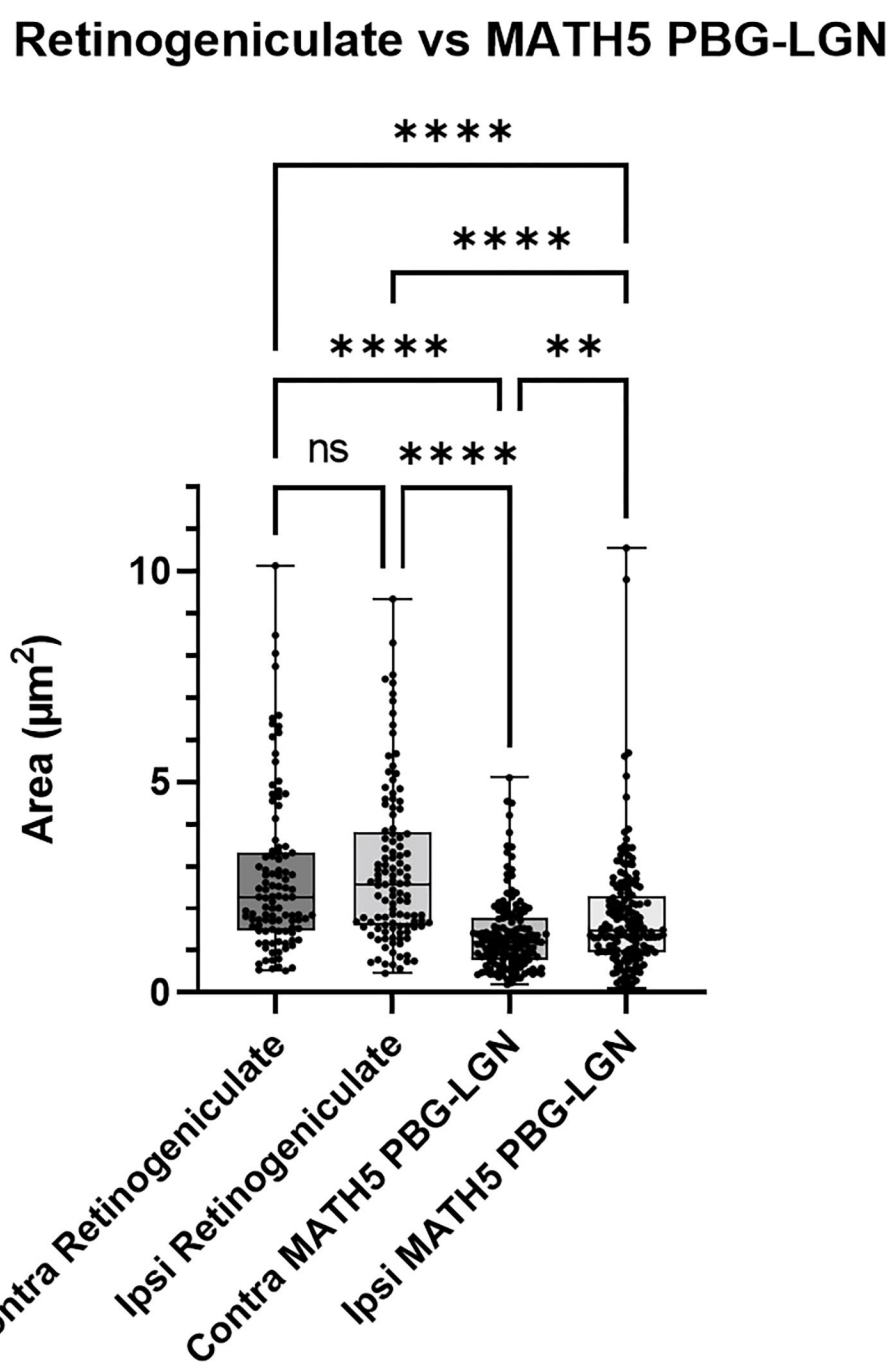

Figure 8:

Retinogeniculate terminals in C57Blk6 (WT) mice are significantly larger than PBG-dLGN terminals in *math5*$^{-/-}$ mice (**** $p < 0.0001$). There is no significant difference in the size of ipsilateral and contralateral retinogeniculate terminals in WT mice (ns). Ipsilateral PBG-dLGN terminals are significantly larger than contralateral PBG-dLGN terminals in *math5*$^{-/-}$ mice (** $p = 0.0083$).

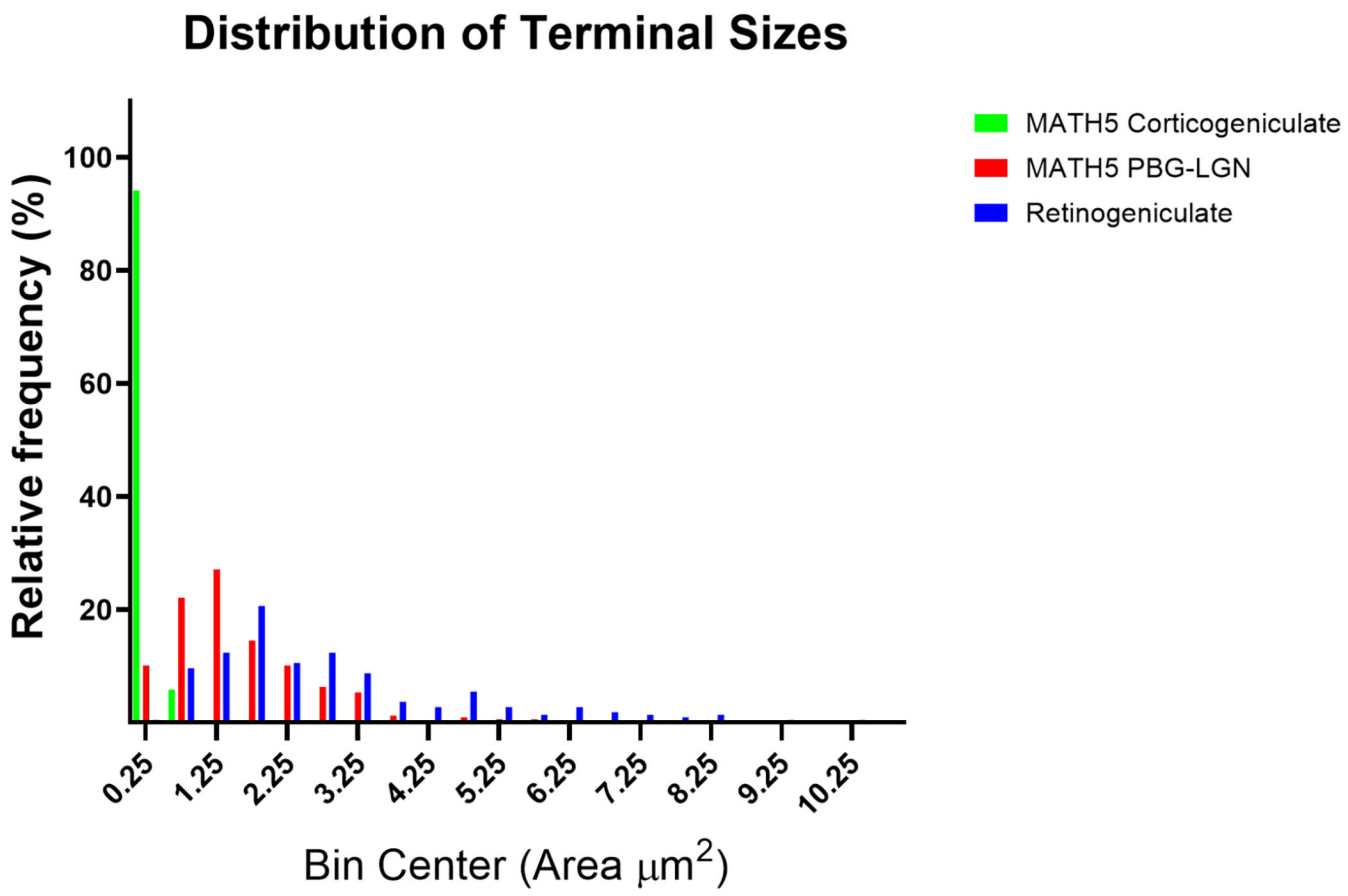

Figure 9:

There is little overlap in the sizes of retinogeniculate terminals in C75Blk6 mice (blue, ipsilateral and contralateral measurements combined) and corticogeniculate terminals in *math5*$^{-/-}$ mice (green). However, there is considerable overlap in the sizes of retinogeniculate terminals in C57Blk6 mice and PBG-dLGN terminals in *math5*$^{-/-}$ mice (red, ipsilateral and contralateral measurements combined).

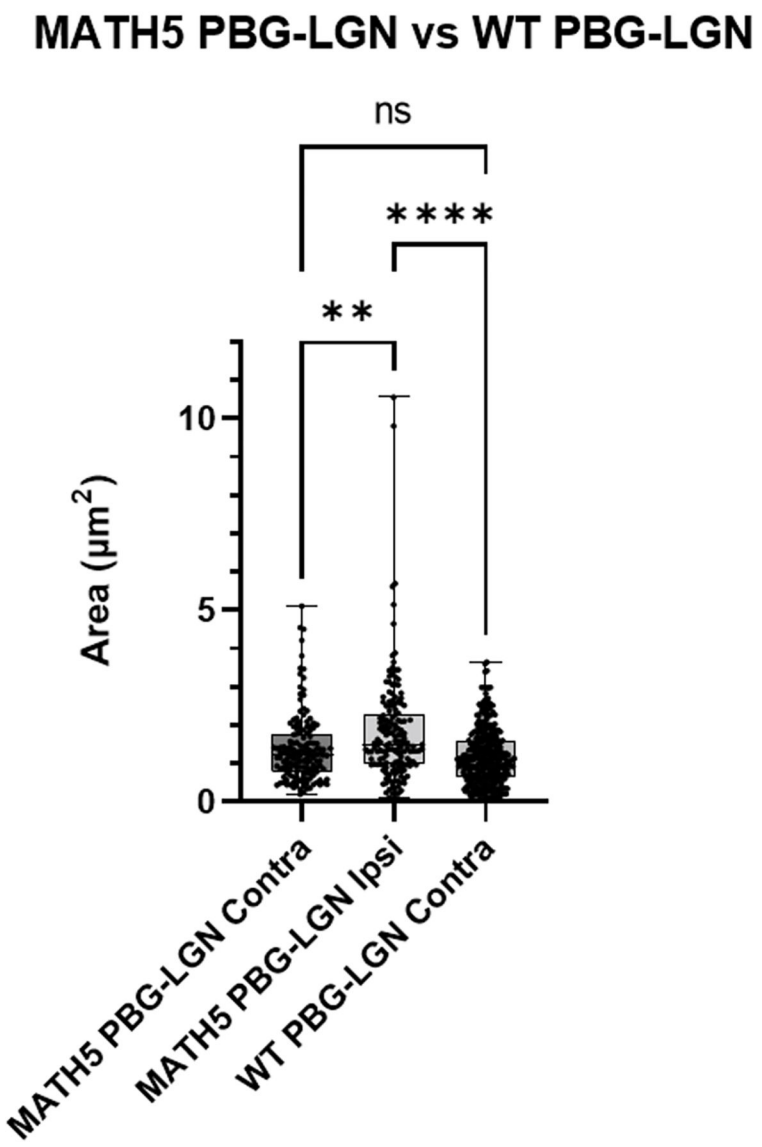

Figure 10:

Ipsilateral PBG-dLGN terminals in *math5*$^{-/-}$ mice are significantly larger than contralateral PBG-dLGN terminals in both C57Blk6 (WT) and *math5*$^{-/-}$ mice (** p = 0.0038; **** p < 0.0001). There is no significant difference between contralateral PBG-dLGN terminals in WT mice and contralateral PBG-dLGN terminals in *math5*$^{-/-}$ mice (ns).